Neurobiology of Disease 130 (2019) 104499

Contents lists available at ScienceDirect

Neurobiology of Disease

journal homepage: www.elsevier.com/locate/ynbdi

Neuronal TDP-43 depletion affects activity-dependent plasticity

Paulina Koza[a], Anna Beroun[a], Anna Konopka[b], Tomasz Górkiewicz[a], Lukasz Bijoch[a], Julio C. Torres[b], Ewa Bulska[b], Ewelina Knapska[c], Leszek Kaczmarek[c,*], Witold Konopka[a,*]

[a] Nencki Institute of Experimental Biology, Polish Academy of Sciences, Warsaw, Poland
[b] Biological and Chemical Research Centre, Faculty of Chemistry, University of Warsaw, Warsaw, Poland
[c] BRAINCITY, Nencki Institute of Experimental Biology, Polish Academy of Sciences, Warsaw, Poland

ARTICLE INFO

Keywords:
TDP-43
AMPA receptors
FLOP/FLIP splice variants
PTZ model

ABSTRACT

TAR DNA-binding protein 43 (TDP-43) is a hallmark of some neurodegenerative disorders, such as frontotemporal lobar degeneration and amyotrophic lateral sclerosis. TDP-43-related pathology is characterized by its abnormally phosphorylated and ubiquitinated aggregates. It is involved in many aspects of RNA processing, including mRNA splicing, transport, and translation. However, its exact physiological function and role in mechanisms that lead to neuronal degeneration remain elusive. Transgenic rats that were characterized by TDP-43 depletion in neurons exhibited enhancement of the acquisition of fear memory. At the cellular level, TDP-43-depleted neurons exhibited a decrease in the short-term plasticity of intrinsic neuronal excitability. The induction of long-term potentiation in the CA3-CA1 areas of the hippocampus resulted in more stable synaptic enhancement. At the molecular level, the protein levels of an unedited (R) FLOP variant of α-amino-3-hydroxy-5-methyl-4-isoxazolepropionic acid receptor (AMPAR) GluR1 and GluR2/3 subunits decreased in the hippocampus. Alterations of FLOP/FLIP subunit composition affected AMPAR kinetics, reflected by cyclothiazide-dependent slowing of the decay time of AMPAR-mediated miniature excitatory postsynaptic currents. These findings suggest that TDP-43 may regulate activity-dependent neuronal plasticity, possibly by regulating the splicing of genes that are responsible for fast synaptic transmission and membrane potential.

1. Introduction

TAR DNA-binding protein 43 (TDP-43) is a ubiquitously expressed, predominantly nuclear protein that was first discovered as a factor that binds to the human immunodeficiency virus-1 TAR DNA sequence and inhibits its transcription (Ou et al., 1995). It is a highly conserved heterogeneous nuclear ribonucleoprotein (hnRNP) that is involved in the regulation of RNA transcription, splicing, and stability (Buratti and Baralle, 2012). The most-described aspect of TDP-43 physiology is its role in alternative splicing. By forming complexes with other hnRNPs, TDP-43 promotes both the exclusion and inclusion of exons in CFTR (Buratti et al., 2004) and apolipoprotein AII (Mercado et al., 2005) mRNA and the inclusion of exons in the transcript of survival motor neuron 2 (SMN-2; Bose et al., 2008). TDP-43 is considered a multifunctional protein because of its broad interactions with DNA, RNA, and proteins (Freibaum et al., 2010; Polymenidou et al., 2011). The nuclear depletion of TDP-43 has also been postulated to lead to the loss of suppression of non-conserved cryptic exon insertion in neurodegenerative diseases (Sun et al., 2017). Research on the neuronal function of TDP-43 intensified when it was identified as a main component of protein aggregates that are typical of frontotemporal lobar degeneration (FTLD) and amyotrophic lateral sclerosis (ALS; Neumann et al., 2006).

The role of TDP-43 in neuronal plasticity was first revealed when it was found to co-localize with FMRP and Staufen-1 in dendrites in depolarized neurons (Wang et al., 2008). Polymenidou et al. (2011) found that low levels of TDP-43 in the murine brain downregulated numerous transcripts of proteins that are involved in synaptic function. TDP-43 depletion in vitro increased the number of dendritic spines and the clustering of α-amino-3-hydroxy-5-methyl-4-isoxazolepropionic acid receptors (AMPARs) at synapses (Majumder et al., 2012). Inefficient AMPA GluA2 subunit editing at the Q/R site was correlated with TDP-43-related pathology that led to excessive Ca^{2+} influx and excitotoxic motor neuron death in cases of sporadic ALS (Aizawa et al., 2010). AMPARs emerged as a potentially main player in the context of TDP-43 dysfunction that leads to aberrant neuronal plasticity.

AMPARs are either homo- or heterotetrameric assemblies of four subunits, GluA1-GluA4. Their stoichiometry in the final receptor

* Corresponding authors.
E-mail addresses: l.kaczmarek@nencki.gov.pl (L. Kaczmarek), w.konopka@nencki.gov.pl (W. Konopka).

https://doi.org/10.1016/j.nbd.2019.104499
Received 11 January 2019; Received in revised form 15 May 2019; Accepted 5 June 2019
Available online 06 June 2019

molecule is the crucial factor that defines channel properties. Additional complexity arises from alternative splicing and nuclear editing processes. AMPAR subunits undergo alternative splicing that leads to the production of FLOP and FLIP variants that affect pharmacological properties and channel desensitization (Sommer et al., 1990). Additionally, three of four subunits (GluA2-GluA4) undergo R/G editing, meaning a codon switch (AGA to GGA [arginine to glycine]) that is positioned in the primary transcript in the exon that directly precedes the FLOP/FLIP module. FLOP and FLIP variants of GluA2-GluA4 transcripts exist in both glycine-edited and arginine-unedited versions, whereas GluA1 only in unedited variant. The efficiency of R/G editing was shown to be correlated with the rate of recovery from desensitization (Lomeli et al., 1994).

Activity-dependent changes in the strength of synaptic connections and excitability of neurons in the network are the basis of memory formation (Daoudal and Debanne, 2003; Kandel et al., 2014). For functional reorganization, neurons employ several mechanisms to integrate nucleus-synapse communication pathways (Cohen and Greenberg, 2008). The expression of genes that are involved in neuronal plasticity is strictly controlled. RNA-binding proteins (RBPs) that regulate splicing, RNA transport, and microRNA-dependent local protein translation have emerged as major players in such nucleus-synapse communication pathways and are able to enhance memory engram formation (Konopka et al., 2010). Global and targeted analyses of putative TDP-43 binding partners suggest its possible role in the regulation of neuronal activity and plasticity (Polymenidou et al., 2011; Tollervey et al., 2011). However, its function in neurons in the context of neuronal physiology and animal behavior is not fully understood. The present study investigated the role of TDP-43 in regulating the expression of pivotal factors in neuronal communication, such as AMPARs.

2. Results

2.1. Novel transgenic rat with neuronal TDP-43 depletion

To study the physiological role of TDP-43, we generated transgenic (TG) rats using the Synapsin-1 promoter to drive the neuron-restricted expression of full-length WT human TDP-43 (Syn–hTDP-43–enhanced green fluorescent protein [eGFP]). The presence of the C-terminal eGFP tag allowed the precise observation of transgene distribution throughout the central nervous system. Microscopic visualization confirmed its primarily nuclear localization in gray matter in the spinal cord (Fig. 1d, e) and brain, including the hippocampus, amygdala, and cortex (Fig. 1a–c).

The level of expression of TDP-43 was first assessed by the Western blot analysis of hippocampal extracts that were obtained from 6-month-old animals. In samples that were collected from TG rats, two bands with molecular weights that corresponded to endogenous TDP-43 (43 kDa) and hTDP-43 fused with eGFP (75 kDa) were detected (Fig. 2b). As previously shown with various TDP-43 TG models, we also observed a significant decrease in endogenous TDP-43 levels in TG rats compared with wildtype (WT) controls. To quantitatively analyze TDP-43 levels, label-free proteomic analyses was performed using ultra-high-performance liquid chromatography coupled with electrospray ionization tandem mass spectrometry (UHPLC-ESI MS/MS). Integrated chromatographic peak areas of all charge states of the registered isotopic patterns were calculated for peptides that differentiated human and rat TDP-43 variants. The relative quantification of peptide that was unique for rats (amino acid sequence: KMDEADASSAVK) confirmed the five-fold depletion of endogenous TDP-43 in TG rats compared with controls (Fig. 2c). The observed phenotype resulted from an auto-regulatory mechanism by which TDP-43 regulates its own expression through direct interactions with the 3′ untranslated region (UTR) of its own transcript (Avendano-Vazquez et al., 2012; Ayala et al., 2011; Polymenidou et al., 2011). Various in vitro and in vivo models demonstrated the importance of physiologically adequate TDP-43 levels in the cell. In the present study, the incorporation of the constitutively expressed hTDP-43 coding sequence into the rat genome decreased endogenous TDP-43 levels. Quantification of the peptide that was common to both rat and human protein (amino acid sequence: TSDLIVLGLPWK), reflecting the total level of TDP-43, revealed 40% lower expression in the hippocampus in TG rats compared with WT controls (Fig. 2b, c). Possibly because of the low copy number of the transgene that was incorporated in the genome (single copy), the expression of an additional copy of TDP-43 was sufficient to lower endogenous protein levels, but this was insufficient to cause an overexpression phenotype (Fig. 2d). Because few animal models with depleted TDP-43 levels have been described to date, we performed a complex analysis of our TG rats.

Histological analyses of sections of the TG rat brain and spinal cord revealed no signs of neurodegeneration or neuroinflammation. We detected no cell loss in either young (6-month-old) or old (1- and 2-year-old) animals. Moreover, the neuronal depletion of TDP-43 did not lead to motor deficits in the rotarod test (Supplementary Fig. S1).

2.2. Improvements in fear memory in Syn–hTDP-43–eGFP transgenic rats followed by alterations of activity-dependent neuronal plasticity

To determine the extent to which TDP-43 depletion affects neuronal function, we first tested its effects on behavioral performance. Six-month-old male rats were subjected to a classical contextual fear conditioning task (Fig. 3a). Conditioned-unconditioned stimulus (CS-US) pairing was introduced in a specific context. In two consecutive test sessions, freezing responses were observed. TDP-43 TG rats exhibited increases in both CS-induced ($p < 0.005$) and context-induced ($p < 0.05$) fear responses (Fig. 3b). These observations suggested that TDP-43-depleted animals developed a stronger CS-US association compared with WT rats. Furthermore, TDP-43-depleted rats also exhibited more efficient context recognition.

Improvements in memory engram formation in TG rats indicated that performance in the behavioral task was consistent with subsequent electrophysiological recordings, indicating an increase in the strength of synaptic connections in TDP-43-depleted neurons. We focused on the CA1 region of the hippocampus because this subregion was shown to be required for the association between a context with an aversive US during fear memory formation (Zhou et al., 2009). Long-term potentiation (LTP) was induced by brief trains of tetanic stimulation (3×100 Hz, 1 s) of CA3 excitatory projections to the CA1 subregion. Field excitatory postsynaptic potential (fEPSP) curves began to vary between groups beginning 40 min after LTP induction and were significantly more stable in TDP-43-depleted rats compared with WT controls (Fig. 3c). To evaluate the basic membrane properties of CA1 neurons, the number of action potentials that were elicited by each applied depolarizing step current was calculated. Whole-cell current-clamp recordings revealed no differences in the number of action potentials between WT and TG animals under baseline conditions. These results suggest that TDP-43 may be engaged in mechanisms that are related to neuronal plasticity. To verify this possibility, we applied a model of neuronal stimulation using the γ-aminobutyric acid-A ($GABA_A$) receptor antagonist pentylenetetrazole (PTZ), which is commonly used to induce activity-induced circuit remodeling. Pentylenetetrazole evokes massive and synchronized neuronal activity. Pentylenetetrazole application reduced the number of action potentials in control neurons, and this reduction was correlated with a higher threshold of action potential firing. Interestingly, a decrease in TDP-43 levels in TG neurons resulted in an inability to homeostatically adjust neuronal excitability (Fig. 3d–g), presumably because of the postulated involvement of TDP-43 in modifying the recovery from the inactivation of voltage-gated sodium and potassium channels (Dong et al., 2014; Xiao et al., 2011). Such a phenomenon following PTZ application did not result in neuronal death in the TG brain (Supplementary Fig. S2).

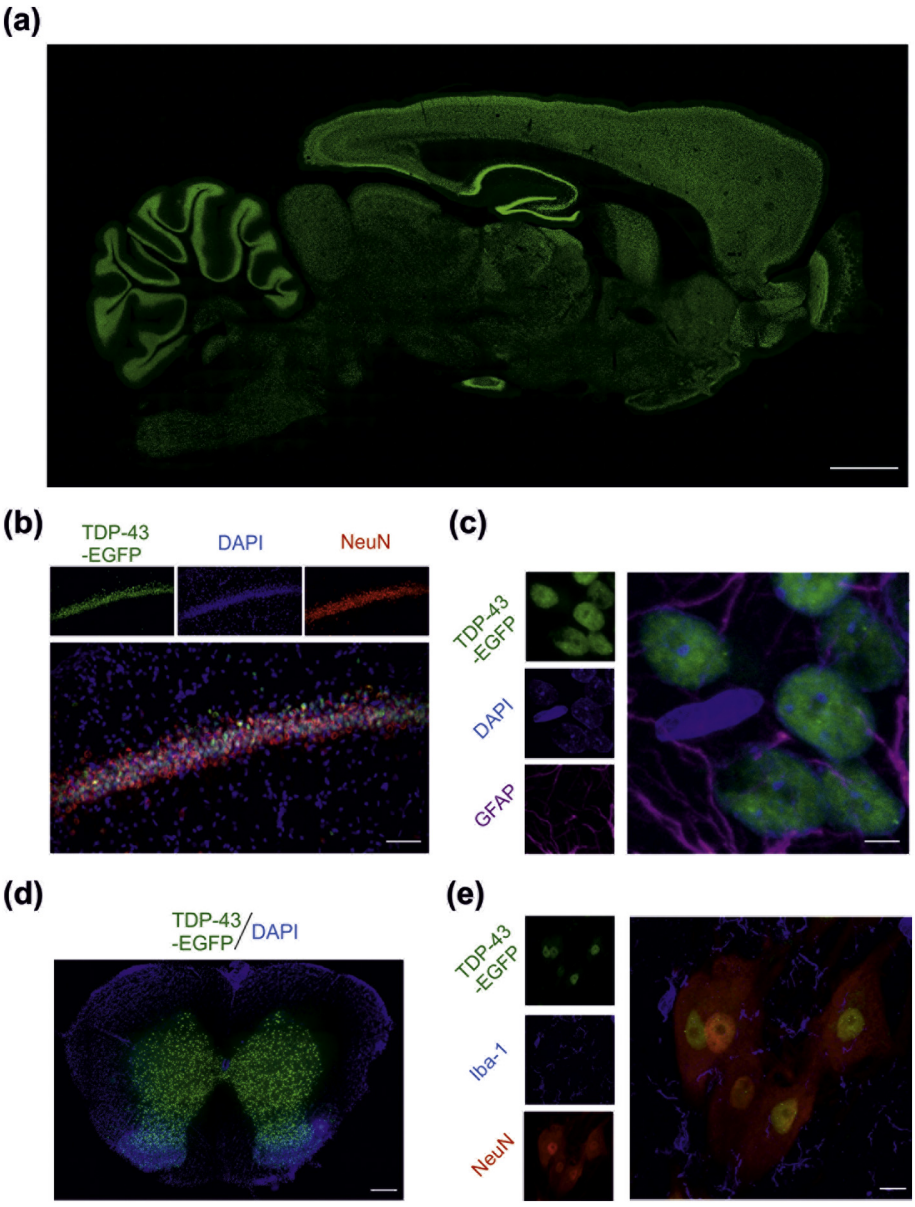

Fig. 1. Syn–hTDP-43–eGFP transgene expression pattern is restricted to neurons in the brain and spinal cord. (a) Synapsin-1 (Syn)-driven hTDP-43-eGFP expression pattern in a sagittal section of the TG rat brain. Scale bar = 3 mm. (b) CA1 region of the hippocampus in a TG rat, immunostained with the neuronal markers NeuN (red) and DAPI (blue). The green fluorescence signal corresponds to eGFP-fused hTDP-43. Scale bar = 50 µm. (c) Primarily nuclear expression of hTDP-43–eGFP in the pyramidal cell layer of the hippocampal CA1 region. Scale bar = 5 µm. (d) Coronal section of the spinal cord of a TG rat where eGFP fluorescence, counterstained with DAPI, is restricted to gray matter of the spinal cord. Scale bar = 250 µm. (e) Spinal motor neurons with nuclear transgene expression, immunostained with the neuronal marker NeuN (red) and microglial marker Iba-1 (blue). Scale bar = 20 µm. (For interpretation of the references to colour in this figure legend, the reader is referred to the web version of this article.)

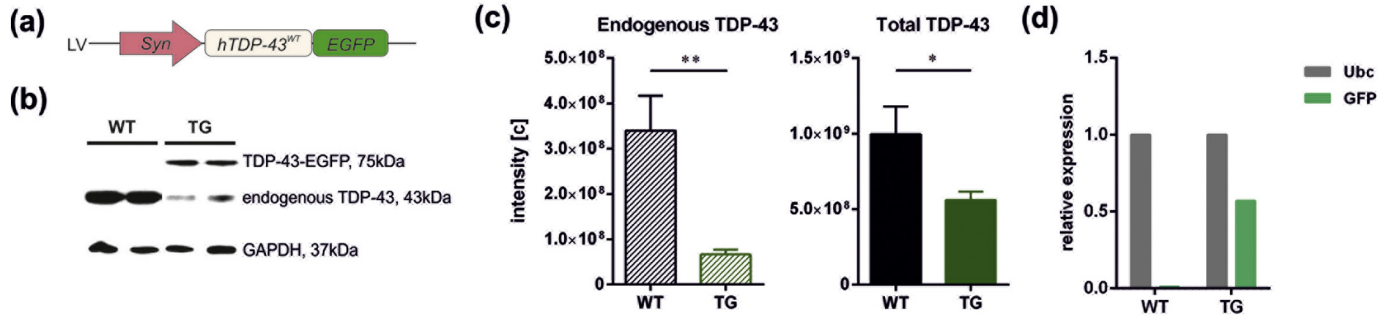

Fig. 2. TDP-43–eGFP and endogenous TDP-43 expression levels. (a) Lentiviral-based construct that was used to generate TG rats. (b) Levels of endogenous and transgene TDP-43 in the TG rat hippocampus compared with controls. GAPDH was used as the loading control. (c) Label-free proteomic quantification of TDP-43 levels in the hippocampus. The data are expressed as the mean analytical signal for peptides that were unique to endogenous rat protein and common for rat and human protein (unpaired *t*-test, endogenous TDP-43, $t = 3.991$, $^{**}p = 0.005$; total TDP-43, $t = 2.5$, $^{*}p = 0.041$). $n = 4$ WT. $n = 5$ TG. (d) Relative expression of GFP transgene transcript compared with reference ubiquitin C transcript. $n = 2$ WT. $n = 2$ TG.

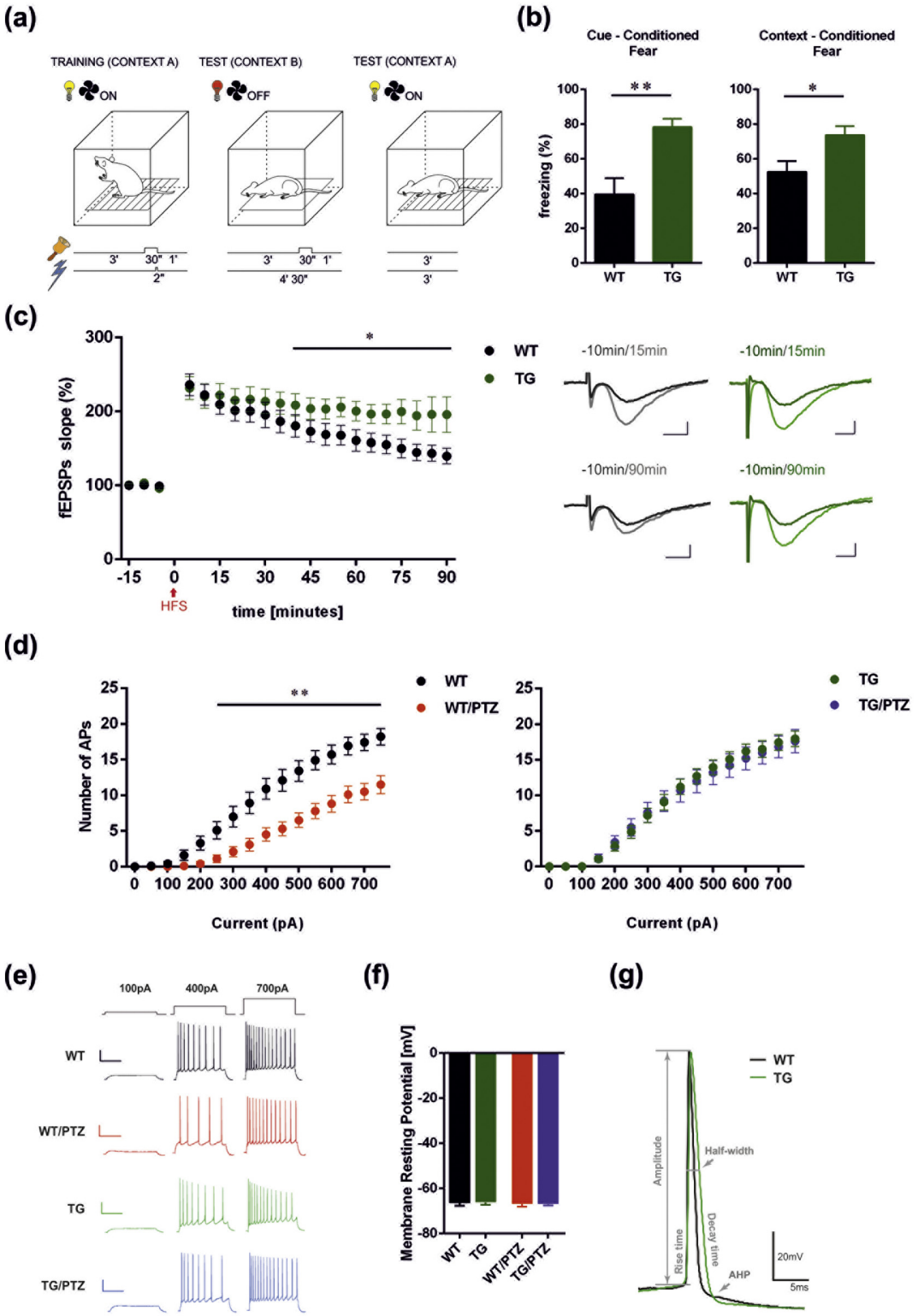

Fig. 3. Fear memory and activity-dependent neuronal plasticity in Syn–hTDP-43–eGFP TG rats. (a) Schematic diagram of stimulus presentation in the classical fear conditioning test. (b) Conditioned responses, presented as a percentage of freezing during 30-s CS presentation in the cue-dependent fear conditioning task and during 3-min context-exposure in the contextual fear conditioning task (unpaired *t*-test: $t = 3.482$, $^{**}p = 0.002$; $t = 2.531$, $^{*}p = 0.02$). $n = 11$ WT. $n = 9$ TG. (c) Long-term potentiation induced by high-frequency stimulation (HFS; 3 × 100 Hz, red arrow) of the Schaffer collaterals (two-way repeated-measures ANOVA; main effect of time: $F_{20,200} = 47.06$, $p < 0.0001$; group × time interaction: $F_{20,200} = 2.485$, $p = 0.0007$; $^{*}p < 0.05$). $n = 5$ WT rats. $n = 7$ WT slices. $n = 5$ TG rats. $n = 5$ TG slices. The right panel shows representative traces of fEPSPs before (−10 min) and after (15 and 90 min) LTP induction. Scale bars = 2 mV and 5 ms. (d) Analysis of the number of action potentials elicited by depolarizing currents (0–700 pA). Whole-cell current-clamp recordings were performed in animals under control conditions and 90 min after pentylenetetrazole (PTZ) stimulation. $n = 14$ WT. $n = 11$ WT/PTZ. $n = 16$ TG. $n = 13$ TG/PTZ (cell based). (e) Example traces of action potential series in response to depolarizing steps of 100, 400, and 700 pA (two-way repeated measures ANOVA; main effect of PTZ treatment in WT: $F_{1,23} = 12.88$, $p = 0.001$). $n = 14$ WT. $n = 11$ WT/PTZ. $^{**}p < 0.01$. Scale bars = 20 mV and 200 ms. (f) CA1 neuron membrane resting potential under control conditions and after PTZ-induced seizures. (g) Overlay of example traces of action potentials in WT and TG neurons. The data are expressed as mean ± SEM. (For interpretation of the references to colour in this figure legend, the reader is referred to the web version of this article.)

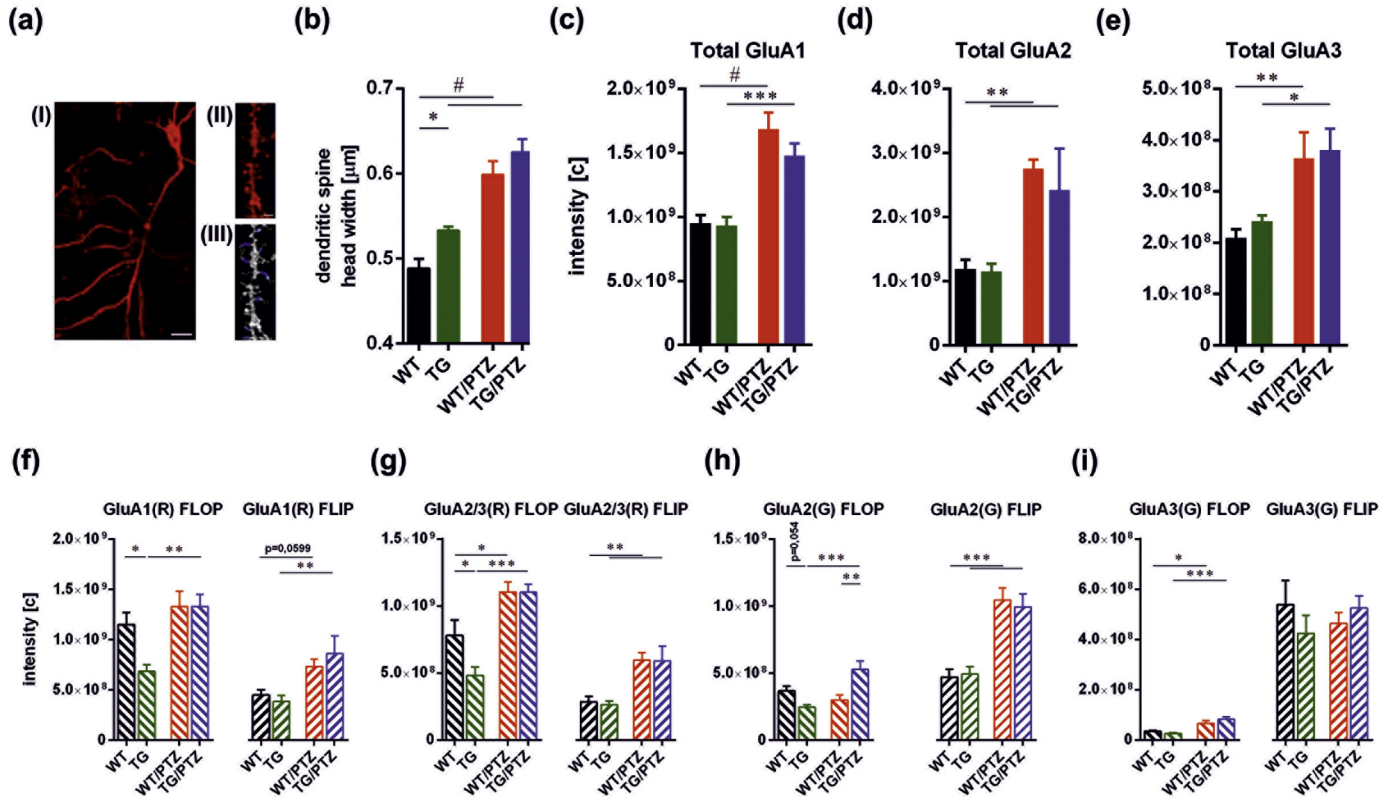

Fig. 4. Dendritic spine size and the expression of AMPAR subunit variants. (a) dendritic spines of CA1 pyramidal neuron stained with DiI (I); dendrite before (II) and after (III) spine morphology analysis with SpineMagick. Scale bar: (I) – 10 µm; (II) 2 µm. (b) Mean dendritic spine head width in CA1 neurons. Spines were visualized by DiI staining under control conditions (n = 5 TG rats; n = 3566 TG spines; n = 5 WT rats; n = 2369 WT spines) and 90 min after PTZ-induced seizures (n = 5 WT/PTZ rats; n = 2324 WT/PTZ spines; n = 5 TG/PTZ rats; n = 2249 TG/PTZ spines; Two-way ANOVA: main effect of PTZ treatment: $F_{1,16} = 64.85$, $p < 0.0001$; main effect of genotype: $F_{1,16} = 8.02$, $p = 0.01$; $^{*}p = 0.022$, WT vs. TG; $^{\#}p < 0.0001$, WT vs. WT/PTZ, TG vs. TG/PTZ). (c-e) Label-free UHPLC MS/MS quantification of peptides that are unique to each AMPAR subunit (GluA1: ADVAVAPLTITLVR; GluA2: YTSALTYDAVQVMTEAFR; GluA3: ADIAVAPLTITLVR). The analysis was performed with samples that were collected under basal conditions and 90 min after PTZ-induced seizures. Two-way ANOVA in (c): main effect of PTZ treatment ($F_{1,15} = 48.67$, $p < 0.0001$; $^{\#}p < 0.0001$, WT vs. WT/PTZ; $^{***}p = 0.001$, TG vs. TG/PTZ). Two-way ANOVA in (d): main effect of PTZ treatment ($F_{1,15} = 23.50$, $p = 0.0002$; $^{**}p = 0.0014$, WT vs. WT/PTZ; $^{**}p = 0.0093$, TG vs. TG/PTZ). Two-way ANOVA in (e): main effect of PTZ treatment ($F_{1,15} = 18.82$, $p = 0.0006$; $^{**}p = 0.004$, WT vs. WT/PTZ; $^{*}p = 0.0129$, TG vs. TG/PTZ). n = 5 WT. n = 5 WT/PTZ. n = 5 TG. n = 4 TG/PTZ. (f-i) Proteomic analysis of peptides that distinguish FLOP and FLIP isoforms of AMPAR subunits and R/G editing status (GluA1[R] FLOP: NPVNLAVLK; GluA1[R] FLIP: GPVNLAVLK; GluA2/3[R] FLOP: NAVNLAVLK; GluA2/3[R] FLIP: TPVNLAVLK; GluA2[G] FLOP: GSSLGNAVNLAVLK; GluA2[G] FLIP: GSSLGTPVNLAVLK; GluA3[G] FLOP: GSALGNAVNLAVLK; GluA3[G] FLIP: GSALGTPVNLAVLK). Pentylenetetrazole-induced changes in levels of FLIP variants of GluA1(R), GluA2/3(R), and GluA2(G) were exclusively treatment- and not genotype-dependent. The levels of the FLOP variant subunits decreased in TG rats under basal conditions and were activity-dependent for GluA1(R) and GluA2(G) only in the TG groups. The levels of the FLOP variant of GluA2/3(R) (which represents the pool of GluA2[R] and GluA3[R], in which the peptide that emerged in the unedited variant upon sample preparation for MS was indistinguishable between the GluA2 and GluA3 subunits) were increased by PTZ in both WT and TG rats, with significantly lower levels in TG rats under control conditions. Both splice variants of the GluA3 subunit were unaffected by TDP-43 depletion. Two-way ANOVA of GluA1(R) FLOP in (f): main effect of PTZ treatment ($F_{1,14} = 12.12$, $p = 0.0037$), main effect of genotype ($F_{1,14} = 3.846$, $p = 0.07$; $^{*}p = 0.0147$, WT vs. TG; $^{**}p = 0.0017$, TG vs. TG/PTZ). Two-way ANOVA of GluA1(R) FLIP in (f): main effect of PTZ treatment ($F_{1,14} = 15.10$, $p = 0.0016$; $p = 0.0599$, WT vs. WT/PTZ; $^{**}p = 0.0039$, TG vs. TG/PTZ). Two-way ANOVA of GluA2/3(R) FLOP in (g): main effect of PTZ treatment ($F_{1,14} = 29.50$, $p < 0.0001$; $^{*}p = 0.029$, WT vs. TG; $^{*}p = 0.0143$, WT vs. WT/PTZ; $^{***}p = 0.0003$, TG vs. TG/PTZ). Two-way ANOVA of GluA2/3(R) FLIP in (g): main effect of PTZ treatment ($F_{1,14} = 24.52$, $p = 0.0002$; $^{**}p = 0.0028$, WT vs. WT/PTZ; $^{**}p = 0.0043$, TG vs. TG/PTZ). Two-way ANOVA of GluA2(G) FLOP in (h): main effect of PTZ treatment ($F_{1,14} = 6.969$, $p = 0.0194$), genotype × PTZ treatment interaction ($F_{1,14} = 18.67$, $p = 0.0007$; $p = 0.0542$, WT vs. TG; $^{***}p = 0.0002$, TG vs. TG/PTZ; $^{**}p = 0.0013$, WT/PTZ vs. TG/PTZ). Two-way ANOVA of GluA2(G) FLIP in (h): main effect of PTZ treatment ($F_{1,14} = 43.27$, $p < 0.0001$; $^{***}p = 0.0003$, WT vs. WT/PTZ; $^{***}p = 0.0005$, TG vs. TG/PTZ). Two-way ANOVA of GluA3(G) FLOP in (i): main effect of PTZ treatment ($F_{1,14} = 26.37$, $p = 0.0002$; $^{*}p = 0.022$, WT vs. WT/PTZ; $^{***}p = 0.0003$, TG vs. TG/PTZ). n = 4 WT in all except (g) where n = 5 WT. n = 5 WT/PTZ; n = 5 TG in all except (g) where n = 4 TG. n = 4 TG/PTZ. The data are expressed as the mean ± SEM intensity of the analytical signal.

2.3. Depletion of TDP-43 increased dendritic spine head size in the hippocampal CA1 area without affecting total levels of AMPAR subunits

The encoding of memory traces is related to dynamic structural modifications of dendritic spines. To investigate whether the increases in fear memory and LTP following TDP-43 depletion resulted from structural alterations, we analyzed dendritic spine morphology in the CA1 area. Dendritic spines were visualized by lipophilic DiI staining. Morphological parameters of dendritic spines were analyzed using semiautomatic SpineMagick software (Ruszczycki et al., 2012), which is used to outline spine contours and calculate spine parameters (i.e., spine length, spine width, neck width, spine circumference, and spine area). For each animal, approximately 500 dendritic spines were analyzed. The data are expressed as mean values for five individuals per group (Fig. 4a). Consistent with the behavioral and electrophysiological results, we observed an approximately 10% increase in spine head diameter (WT, 0.488 ± 0.011 µm; TG, 0.533 ± 0.004 µm; $p < 0.05$) of TG CA1 pyramidal neurons (Fig. 4b). We did not observe other alterations of basic spine parameters. The increases in dendritic spine area and circumference as a consequence of head widening were

considered a derived feature and are not shown here. Dendritic spine head enlargement that is induced by an increase in neuronal activity is interpreted as a process that leads to the strengthening of synaptic connections. Pentylenetetrazole-induced seizure episodes resulted in the further enlargement of spine head width. These changes were exclusively treatment- and not genotype-dependent. Interestingly, spine head width that distinguished groups under basal conditions reached similar values between groups 90 min after seizure induction, indicating the same physiologically controlled spine growth potential in both groups of animals (20% growth in WT, 17% growth in TG; Fig. 4b).

The process by which dendritic spine enlargement is correlated with an increase in synaptic strength is strictly related to an increase in the number of AMPARs (Matsuzaki et al., 2004). The incorporation of this group of receptors at CA1 synapses is crucial for the expression of contextual fear conditioning (Mitsushima et al., 2011). Thus, we used a label-free UHPLC-ESI MS/MS-based proteomic approach that allowed us to distinguish and quantify unique peptides for each AMPAR subunit. We focused on GluA1, GluA2, and GluA3 because they are the most abundant subunits in the hippocampus. The growth of dendritic spines in WT and TG neurons after seizure induction was associated with a quantitative increase in the total level of GluA1-A3 subunits in the hippocampus. We did not detect differences in total AMPAR subunit levels between WT and TG rats (Fig. 4c–e).

2.4. Alterations of the ratio of alternatively spliced AMPAR FLOP/FLIP variants in TDP-43 transgenic neurons

The functional diversity of AMPARs arises from receptor subunit composition. Each AMPAR subunit is subjected to the alternative splicing of mutually exclusive FLOP and FLIP exons. This affects the ion-conducting properties of the receptor. Moreover, FLOP and FLIP variants of GluA2-GluA4 transcripts exist in either arginine (*R*)-unedited or glycine (G)-edited versions. FLOP and FLIP protein isoforms differ in 9–11 amino acids, depending on the subunit (Sommer et al., 1990). We found that TDP-43 depletion altered the subunit composition of glutamatergic AMPARs, mostly the FLOP splice variant (Fig.4f-i). For GluA1(R), GluA2/3(R), and GluA2(G), levels of the FLOP variant decreased under basal conditions. The FLIP variant for all subunits was unaffected by TDP-43 depletion both under basal conditions and following PTZ application. The changes that were observed for GluA3(G) were genotype-independent. The ratio of FLOP/FLIP isoforms of GluA1(R), GluA2/3(R), GluA2(G) decreased upon PTZ stimulation in controls, whereas the ratio remained constant in the TG hippocampus (Fig. 5a–d), which was predominantly a result of lower levels of the FLOP isoform.

2.5. Cyclothiazide slows mEPSC decay in TDP-43-depleted pyramidal neurons

FLIP and FLOP splice variants of AMPARs differ in their channel properties, such as channel opening, deactivation, and desensitization (Mosbacher et al., 1994; Pei et al., 2009; Sommer et al., 1990), which has a profound impact on receptor kinetics. To determine whether changes in the contributions of FLIP/FLOP splice variants that were observed in TDP-43 TG neurons affect the synaptic function of AMPARs, we performed whole-cell recordings of neurons in the CA1 region of the hippocampus (Fig. 5e-f). We analyzed the decay time of AMPAR-mediated miniature excitatory postsynaptic currents (mEPSCs) to investigate the receptor deactivation time. We then applied 100 μM cyclothiazide (CTZ). Cyclothiazide is a positive AMPAR modulator that preferentially binds to FLIP variants and blocks channel deactivation and desensitization (Fucile et al., 2006; Partin et al., 1996, 1994; Taschenberger et al., 2002). In neurons with TDP-43 depletion, we observed a slower decay time of AMPAR mEPSCs (WT: 13.62 ± 0.41 ms, $n = 9$; TG: 16.48 ± 0.88 ms, $n = 12$, $p = 0.01$, *t*-test), suggesting different contributions of different AMPAR splice variants. Cyclothiazide had no effect on the kinetics of AMPARs in WT cells (15.12 ± 1.07 ms, $n = 15$, $p = 0.23$, paired *t*-test). Pentylenetetrazole-induced seizures, however, led to a change in the synaptic properties of AMPARs, reflected by a longer mEPSC decay time (WT/PTZ: 15.93 ± 1.26 ms; WT/PTZ + CTZ: 19.12 ± 1.25 ms, $n = 6$, $p = 0.005$, paired *t*-test). In TG neurons, CTZ application prolonged the decay time, but this effect was not observed in neurons from PTZ-treated rats (TG + CTZ: 19.38 ± 0.71 ms, $n = 12$, $p < 0.001$, paired *t*-test).

2.6. TDP-43 transgenic synapse 50-Hz burst responses in CA1 pyramidal neurons

To investigate the way in which the contribution of different splice variants in TDP-43 TG neurons affects synaptic function during repetitive, high-frequency stimulation (HFS), we recorded 50-Hz trains of EPSCs. Such burst responses in the hippocampus represent the physiological function of AMPARs because high-frequency activity is necessary to induce LTP in CA3-CA1 synapses. We recorded a train of nine stimulations at 50 Hz and normalized the consecutive amplitudes to the first response (Fig. 6a). In a burst of nine pulses, WT neurons exhibited a profound 40% decrease in the amplitude of consecutive peaks, suggesting that a fraction of AMPARs entered the desensitized state with each repeated stimulation. In the presence of CTZ, which blocks receptor desensitization, the decrease in consecutive peak amplitudes was smaller (amplitudes of the ninth peak: WT: 0.59 ± 0.04, WT + CTZ: 0.80 ± 0.09). Trains of EPSCs that were recorded from TDP-43 TG neurons were unaffected by the application of CTZ, but the decrease in consecutive peak amplitudes was greater (65%) compared with WT cells (amplitudes of the ninth peak: TG: 0.35 ± 0.04, TG + CTZ: 0.38 ± 0.03; $p = 0.0005$, WT vs. TG; unpaired *t*-test: $t = 3.985$). These results suggest that AMPARs in TG neurons do not enter the desensitized state, but CTZ still affects their deactivation time, reflected by a longer decay time that was measured for the ninth peak of the 50-Hz train (Fig. 6b; WT: 11.967 ± 0.52 ms; WT + CTZ: 12.576 ± 0.463 ms, $n = 15$; TG: 12.377 ± 0.633 ms; TG + CTZ: 14.385 ± 0.66 ms, $n = 11$).

3. Discussion

The present study evaluated a novel TG rat model with the neuron-restricted depletion of TDP-43, which is involved in the regulation of RNA metabolism and neurodegeneration. The results suggested that TDP-43 may regulate neuronal activity. TDP-43 depletion led to quantitative alterations of alternatively spliced FLOP and FLIP variants of AMPAR subunits.

Transgenic Syn–TDP-43–eGFP rats were characterized by the depletion of TDP-43 levels in neurons. This phenotype was achieved by introducing into the rat genome cDNA that encodes hTDP-43 driven by the Synapsin-1 promoter, which resulted in an overall decrease in endogenous TDP-43. This downregulation of TDP-43 that resulted from the incorporation of additional copies of TDP-43 into the genome was previously reported in other in vivo models (Igaz et al., 2011; Swarup et al., 2011; Xu et al., 2010), reflecting the autoregulatory properties of TDP-43 (Ayala et al., 2011; Polymenidou et al., 2011). Using a proteomics approach, we found that a constitutively active transgene that lacked the *TARDBP* regulatory 3′ UTR was sufficient to obtain a model with lower levels of total TDP-43. The lentiviral transgenesis method that we utilized facilitated the generation of a stable TG line with a low copy number of the transgene. In TDP-43 TG animals, the expression of an FTD/ALS phenotype has been shown to be directly proportional to the level of TDP-43 in the cell (Wils et al., 2010; Wu et al., 2012; Yang et al., 2014). When TDP-43 levels are only slightly elevated, no degenerative symptoms are observed. Relatively few models that are characterized by TDP-43 depletion have been described to date. The

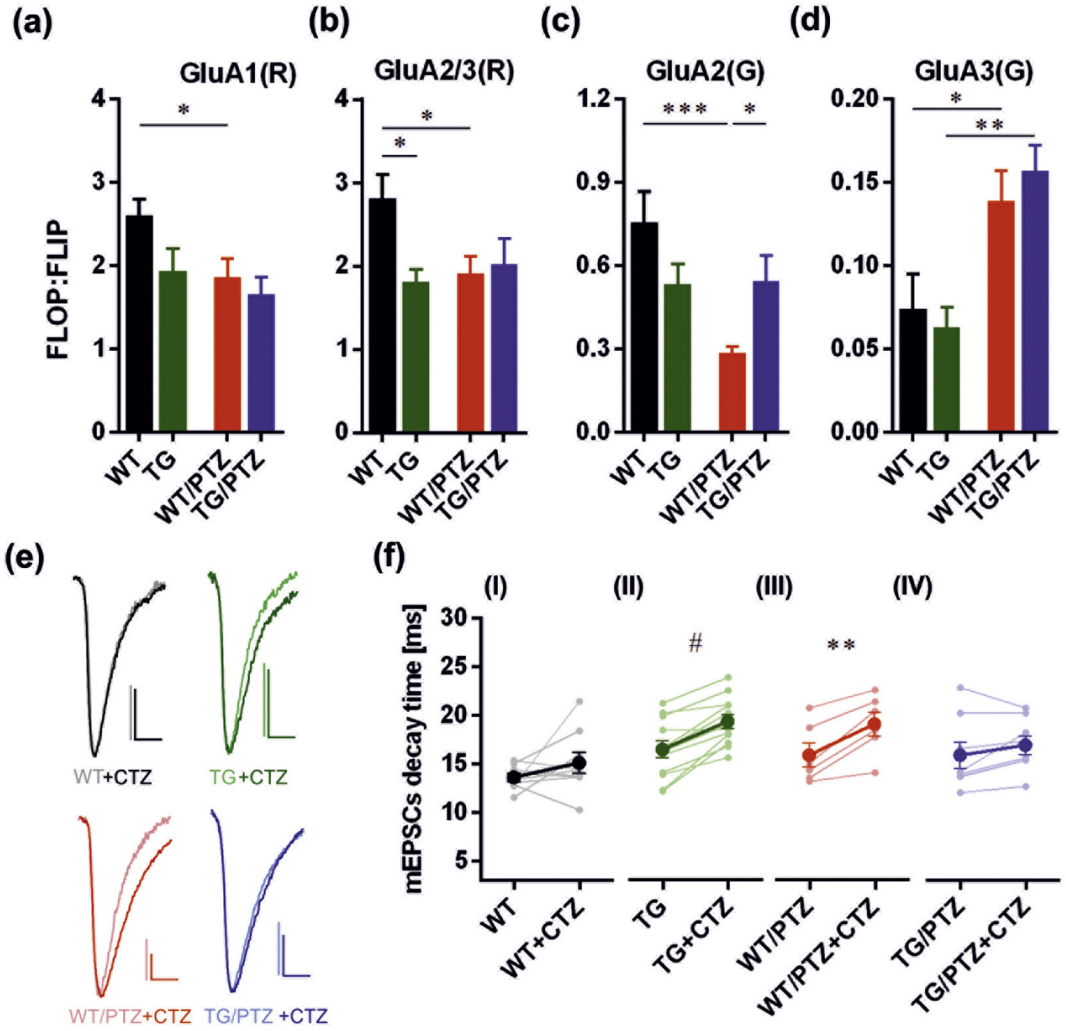

Fig. 5. FLOP/FLIP AMPAR subunit ratios in total protein extracts from the hippocampal formation and influence of CTZ on channel properties. (a-d) Level of alternatively spliced FLOP and FLIP AMPAR subunit variants upon seizure induction. The data are expressed as the mean ± SEM analytical signal ratios for peptides that are unique to FLOP/FLIP isoforms and R/G editing status. In WT rats, PTZ-induced seizures resulted in a decrease in the FLOP/FLIP ratio of (a) GluA1(R), (b) GluA2/3(R), and (c) GluA2(G). Following TDP-43 depletion, the FLOP/FLIP ratios of these subunits were unaltered after PTZ application but decreased under basal conditions. Two-way ANOVA in (a): main effect of PTZ treatment ($F_{1,14} = 4.785$, $p = 0.0462$; $^{*}p = 0.04$, WT vs. WT/PTZ; $p = 0.06$, WT vs. TG). Two-way ANOVA in (b): treatment × genotype interaction ($F_{1,14} = 4.947$, $p = 0.0431$; $^{*}p = 0.0166$, WT vs. WT/PTZ; $^{*}p = 0.0133$. WT vs. TG). Two-way ANOVA in (c): main effect of PTZ treatment ($F_{1,14} = 8.942$, $p = 0.009$), treatment × genotype interaction ($F_{1,14} = 9.984$, $p = 0.007$; $^{***}p = 0.0007$, WT vs. WT/PTZ; $^{*}p = 0.03$, WT/PTZ vs. TG/PTZ; $p = 0.059$, WT vs. TG). The changes in the GluA3(G) FLOP:FLIP ratio in (d) were exclusively treatment-dependent. Two-way ANOVA in (d): main effect of PTZ treatment ($F_{1,14} = 22.44$, $p = 0.0003$; $^{*}p = 0.016$, WT vs. WT/PTZ; $^{**}p = 0.0014$, TG vs. TG/PTZ). $n = 4$ WT in (a), (c), and (d). $n = 5$ WT in (b). $n = 5$ WT/PTZ. $n = 5$ TG in (a), (c), and (d). $n = 4$ WT/PTZ in (b). $n = 4$ TG/PTZ. (e-f) Electrophysiological verification of alteration of FLOP/FLIP composition in CA1 neurons. The mEPSC decay time was analyzed in the presence of CTZ (100 μM). (e) Examples of averaged mEPSC events, peak-scaled to traces before CTZ application. Scale bars = 5 pA and 10 ms. (f) Plots of the effect of CTZ on mEPSC decay time under control conditions (I, II) and upon seizure induction (III, IV). The data are expressed as individual cell responses (pale colors) and mean ± SEM (bold line). The mEPSC decay time decreased upon CTZ application in WT PTZ-treated rats and control TG rats (paired *t*-test: WT, $t = 1.306$, $p = 0.22$, $n = 9$; TG, $t = 6.063$, $^{\#}p < 0.0001$, $n = 12$; WT/PTZ, $t = 4.698$, $^{**}p = 0.005$, $n = 6$; TG/PTZ, $t = 1.695$, $p = 0.133$, $n = 8$).

generation of global TDP-43 knockouts was shown to be impossible (Sephton et al., 2010; Wu et al., 2010). The deletion of one allele of the TDP-43 gene did not alter protein levels (Chiang et al., 2010; Sephton et al., 2010; Wu et al., 2010). Conditional TDP-43 knockout animals die just a few days after mutation induction, with no signs of the development of FTD/ALS symptoms (Chiang et al., 2010). No TG rats with TDP-43 depletion have been previously generated. In the present study we generated TDP-43 TG rats that did not develop neurodegenerative symptoms or express motor deficits.

We first tested the effects of TDP-43 neuronal depletion on animal behavior and observed improvements in cognitive function, reflected by an increase in the acquisition of fear memory. In the classical fear conditioning paradigm, TG rats exhibited increases in freezing responses to both the cue and context. Fear conditioning is widely used to investigate learning and memory. In brain regions that are involved in memory trace encoding (e.g., hippocampus and amygdala), rearrangements of neuronal circuits and dynamic modifications of dendritic spines occur (Konopka et al., 2011). The acquisition of fear memory is strictly related to increases in glutamatergic transmission and synaptic modifications (Ostroff et al., 2010; Zhou et al., 2009). Our initial results prompted us to investigate the contribution of TDP-43 to neuronal plasticity, which has been previously suggested (Wang et al., 2008). To verify that the TDP-43 depletion-induced increase in fear memory was related to structural alterations, we analyzed dendritic spines morphology in the CA1 area of the hippocampus. The CA1 subregion is required for the association between a context and an

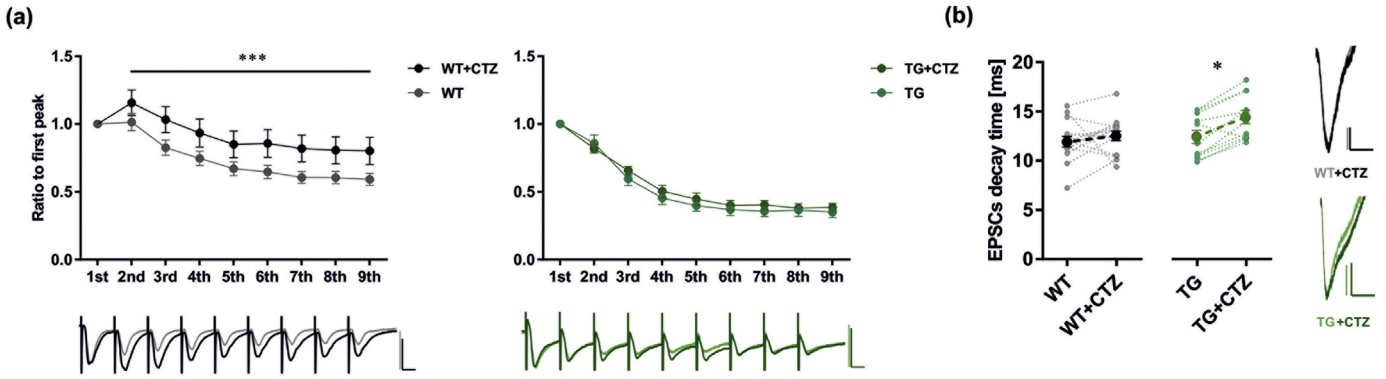

Fig. 6. Effects of CTZ on burst responses in CA pyramidal neurons. (a) Example traces and normalized, averaged amplitudes of nine consecutive EPSC peaks in response to 50-Hz train stimulation. The application of CTZ increased the amplitudes of consecutive peaks in WT neurons (two-way repeated-measures ANOVA; main effect of CTZ, $F_{1,14} = 5.371$, $p = 0.036$; $^{***}p \leq 0.0001$, WT vs. WT + CTZ). $n = 15$ WT. $n = 12$ TG (cell based). Scale bars = 100 pA and 10 ms. (b) Example traces and plots that show the effect of CTZ on the ninth EPSC amplitude decay time in control WT and TG neurons. The data are expressed as individual cell responses (pale colors) and mean ± SEM (bold dashed line). The application of CTZ prolonged the response decay time in TG neurons (unpaired *t*-test: $t = 2.093$; $^{*}p = 0.049$, TG vs. TG + CTZ). $n = 15$ WT. $n = 11$ TG. Scale bars = 50 pA and 25 ms.

aversive US (Kim and Fanselow, 1992; Zhou et al., 2009). Previous studies showed that TDP-43 depletion affected spinogenesis and caused AMPAR clustering at the synapse (Majumder et al., 2012). In the present study, we observed an increase in spine head width in TG CA1 neurons. Activity-dependent changes in the efficacy of synaptic transmission are a basic feature of many excitatory synapses. The most extensively studied model of activity-dependent synaptic plasticity is the LTP of glutamatergic synapses. In the Syn–hTDP-43 model, instead of an enhancement of LTP, we observed an extended duration of LTP. The increase in synaptic transmission is generally attributable to postsynaptic modifications of AMPARs with regard to their number and kinetic properties (Benke et al., 1998; Yang et al., 2008). However, another possible explanation is an increase in the lateral diffusion of receptors that allows for the fast exchange of desensitized receptors to sustain the enhancement of transmission. Blocking surface diffusion in CA1 neurons strongly attenuates the expression of LTP and contextual fear learning (Penn et al., 2017). Nevertheless, the direct involvement of TDP-43 in the regulation of AMPAR translocation requires further investigation.

The most important observation in the present study, confirmed by examinations of electrophysiological properties of AMPARs, was the reduction of the protein levels of FLOP variants of AMPAR subunits in TDP-43 TG neurons. Although the mechanism of this reduction remains to be determined, TDP-43 may be engaged in regulating the alternative splicing of AMPAR transcripts. Interactions between TDP-43 and AMPAR subunit mRNA have been previously reported (Sephton et al., 2011). TDP-43 also appears to be engaged in RNA transport. With regard to splice variant and R/G editing status, previous studies suggested that different GluA subunit mRNAs are transported along dendrites with different efficiency (La Via et al., 2013). The postulated correlation between TDP-43 and inefficient GluA2 R/G editing (Aizawa et al., 2010) was investigated at the RNA level. In the present study, no changes were detected when the entire hippocampal formation was analyzed. However, we detected alterations of a number of micro RNAs in Syn–hTDP-43 rats that may regulate the translation of AMPAR mRNAs (data not shown). The lower levels of AMPAR FLOP variants may be a result of previously reported homeostatic responses of neuronal network activity (Balik et al., 2013; Penn et al., 2012) or the disruption of endoplasmic reticulum-mitochondrion interactions (Coleman et al., 2010; Gautam et al., 2019), independent of a direct influence of TDP-43 on AMPAR mRNA.

Modifications of AMPAR subunit composition and the differential expression of alternative splice variants have a profound impact on receptor kinetics. Based on the amount of current that passes through the channel and the channel's ability to quickly exit the desensitized state, AMPARs predispose the synapse to maintaining fast synaptic transmission and facilitate synaptic plasticity. In the present study, we examined the way in which TDP-43 depletion affects the function of AMPARs in the CA1 region of the hippocampus. The analysis of decay time kinetics of mEPSCs indicated that TG neurons expressed AMPAR splice variants that deactivated at a slower rate; hence, they passed more current for each synaptic response. TDP-43 TG synapses appeared to exhibit an enhancement of basal synaptic transmission. Application of the AMPAR positive allosteric modulator CTZ was reported to have no effect on CA1 AMPARs (Arai and Lynch, 1998). The present results showed no difference in AMPAR decay kinetics in WT neurons. However, 1.5 h after PTZ-induced seizures, newly modified AMPARs were incorporated into the synapse. Although their basal kinetics did not differ from WT AMPARs before seizure induction, CTZ application revealed their higher propensity to deactivate. The CTZ-induced lengthening of AMPAR mEPSC decay time in TG neurons suggested that these synapses were already saturated with splice variants of AMPARs that were different from WT neurons. Our electrophysiological recordings of 50-Hz burst responses further supported this observation. The application of CTZ had no effect on the amplitudes of subsequent peaks in TG neurons, suggesting no contribution of desensitization to the short-term plasticity shaping high frequency stimulation responses. Several processes affect the magnitude of consecutive peaks in a train of responses, such as presynaptic release probability, desensitization, and the lateral diffusion of AMPARs (Chen et al., 2002; Fioravante and Regehr, 2011; Heine et al., 2008). After excluding the possible contribution of desensitization to the reduction of AMPAR consecutive peak amplitudes, the reduction of lateral diffusion may explain the observed phenomenon. Alternative splice variants of AMPARs bind to their auxiliary subunits with different affinity, which can affect their mobility in the synapse (Cais et al., 2014; Constals et al., 2015). One possibility is that AMPARs in TG neurons exhibit a decrease in lateral diffusion. Therefore, the synapse is filled with closed, desensitized, or saturated receptors for a longer period of time. However, CTZ, which prevents desensitization, did not rescue the reduction of burst peak amplitudes. The lack of an effect of CTZ suggests that lateral diffusion increased, thus allowing the rapid removal of desensitized receptors from the synapse (Constals et al., 2015) and precluding the effect of CTZ. The most probable explanation for the reduction of burst peak amplitudes appears to be an increase in presynaptic release probability, which causes depletion of the readily releasable pool of vesicles, of TG synapses compared with WT neurons.

Previous electrophysiological studies that analyzed outside-out patches from recombinant AMPARs provided data on the way in which CTZ differentially affects channel kinetics based on different splice

variants of each subunit (GluR1–4). Cyclothiazide preferentially binds to FLIP variants of AMPARs (Partin et al., 1994), blocks desensitization, and stabilizes the receptor in a non-desensitized state (Fucile et al., 2006). The lack of an effect of CTZ may be attributable to a higher abundance of FLOP variants in the synapse of TG neurons, but such a conclusion should be drawn with caution because CA1 synaptic AMPARs comprise various subunits and splice variants. Nonetheless, CTZ belongs to a group of substances called "ampakines" that reduce AMPAR deactivation and desensitization, enhance the amplitude of currents, and facilitate LTP (Arai and Kessler, 2007; Yamada, 1998). Many rodent and human studies confirmed the role of ampakines as cognitive enhancers (Granger et al., 1993; Hampson et al., 1998; Ingvar et al., 1997; Lynch and Gall, 2006; Lynch et al., 1996). The recordings of AMPAR currents in TDP-43 TG neurons in the present study suggest that TG synapses possess AMPARs with enhanced properties. This enhancement of synaptic properties improved learning at the behavioral level and facilitated LTP, improved channel currents, and resulted in resistance to desensitization at the cellular level.

In summary, the present study showed that TDP-43, which is involved in many aspects of RNA processing, may control both synaptic and non-synaptic neuronal plasticity. Our results indicated that the AMPAR FLOP isoform was the most affected by TDP-43 depletion. Changes in AMPAR composition strengthened synaptic connections, resulting in improvements in fear memory formation. The pharmacological manipulation of AMPAR kinetics may exert similar effects on cognitive enhancement (Lynch and Gall, 2006). However, further studies are required to uncover possible limitations of the glutamate-evoked enhancement of AMPAR transmission that leads to beneficial effects on neuronal networks but not to cell death that can be caused by glutamate excitotoxicity (Figiel and Kaczmarek, 1997).

4. Experimental procedures

4.1. Generation of Syn–hTDP-43^{WT} rats

cDNA that encoded human WT TDP-43 (TDP-43^{WT}) with a C-terminal eGFP tag (provided by Jane Wu, Northwestern University, Feinberg School of Medicine, Chicago, IL, USA) was cloned under the neuron-specific Synapsin-1 promoter into the lentiviral pTRIP plasmid. Lentiviral vectors were prepared as described previously (Bieganska et al., 2012) and subsequently used for sub-zonal injections into pronuclear stage Wistar rats zygotes. Transgenic founders were identified by polymerase chain reaction (PCR) using the following primers: TDP-43 (forward, GGTATGATGGGCATGTTAGC) and eGFP (reverse, CGTC GCCGTCCAGCTCGACCAG). These founders were bred with WT animals to establish the stable TG line.

The animals were housed under a 12 h/12 h light/dark cycle. Food and water were available ad libitum. All of the animals that were used in the experiments were bred in heterozygous pairings. Wildtype littermates of Syn–hTDP-43^{WT} TG rats were used as controls. All of the procedures were performed in accordance with European law and approved by the Local Ethics Committee for Animal Experimentation.

4.2. Immunofluorescence

For brain isolation, the rats were pre-sedated with an intraperitoneal injection of 75 mg/kg ketamine and 0.5 mg/kg medetomidine, deeply anesthetized with Morbital (150 mg/kg; 26.7 mg/ml pentobarbital, 133.3 mg/ml sodium pentobarbital), and transcardially perfused with ice-cold phosphate-buffered saline (PBS; pH 7.4) followed by 4% paraformaldehyde (PFA) in PBS (pH 7.4). Brains were removed and post-fixed for 24 h in 4% PFA. For subsequent immunofluorescent staining, the brains were incubated in 30% sucrose in PBS and cryosectioned (30 µm serial sagittal and coronal sections, Leica). The following antibodies were used: NeuN (1:500; Abcam), GFAP (1:500; Sigma), Iba-1 (1:500; Abcam), and DAPI (Fluoromount-G, Sothernbiotech).

4.3. Immunoblotting

To prepare protein lysates, the animals were anesthetized with isoflurane (Baxter), and brains were isolated. The hippocampal formation was separated and homogenized in ice-cold glass tissue homogenizers in 1% sodium dodecyl sulfate (SDS) solution with protease inhibitor cocktail (cOmplete EDTA free, Roche). The samples were incubated at 95 °C for 10 min and centrifuged at 12,000 ×*g* at 4 °C for 10 min. Supernatants were collected and stored at -80 °C. Before further analysis, proteins were denatured for 5 min in 98 °C in sample buffer (20% glycerol, 4% SDS, 0.04% bromophenol blue, and 250 mM Tris-HCl, pH 6,8) with 5% β-mercaptoethanol (v/v). Sodium dodecyl sulfate-polyacrylamide gel electrophoresis (SDS-PAGE) and semi-dry transfer to polyvinylidene difluoride membranes (0.45 µm, Immobilon-P, Millipore) were performed according to standard protocols. The following antibodies were used: TDP-43 (1:1000; Proteintech) and GAPDH (1:10,000; Millipore).

4.4. Label-free quantitative proteomics

Tissue lysates were prepared as described above. A total of 0.9 mg of hippocampal formation proteins was separated by 10% SDS-PAGE. Proteins were stained with colloidal Coomassie Blue solution (Roti-Blue, Carl Roth) according to the standard protocol. Excised gel bands that corresponded to the molecular weight of AMPARs (~100 kDa), endogenous TDP-43 (43 kDa), and TDP-43/GFP transgene (75 kDa) were cut into 1 mm^3 pieces and destained with 30% acetonitrile (ACN; Millipore)/70% 100 mM NH_4HCO_3 (Sigma). The gel pieces were then dehydrated with 50% ACN/0.1% trifluoroacetic acid (TFA; Sigma) and dried in a vacuum concentrator (SpeedVac, Eppendorf). To reduce disulfide bridges and protect free –SH groups, the samples were treated with 10 mM dithiothreitol (DTT; Sigma) in 100 mM NH_4HCO_3 and with 55 mM iodoacetamide (IAA; Sigma) in 100 mM NH_4HCO_3, respectively. The gel pieces were then washed with 100 mM NH_4HCO_3, dehydrated with ACN, and dried in a vacuum concentrator. The gel pieces were rehydrated with 25 µg/ml trypsin solution (Trypsin Gold, MS Grade, Promega) in 40 mM NH_4HCO_3/10% ACN and incubated at 37 °C overnight. Peptides were extracted with 5% formic acid (FA; Sigma) and ACN. Samples were concentrated in a vacuum concentrator until dry and resuspended in 0.1% aqueous FA before further analysis.

Peptide samples were analyzed using the nanoAquity UHPLC system (Waters) coupled to a Q Exactive mass spectrometer (Thermo Scientific) that was equipped with an ESI source. The following conditions were used for UHPLC: BEH130 C18 column, 75 µm × 250 mm, 3 µm particle size (Waters). Peptides were separated using a gradient elution method from 5% to 50% ACN that contained 0.1% FA within 180 min. Mass spectrometry spectra were acquired at a resolving power of 70,000 within a mass range of 350–2000 m/z. For the fragmentation of precursor ions, HCD activation was applied. The mass spectra files were processed using the Mascot search engine (Matrix Science, London, UK) using UniProtKB/Swiss-Prot and Trembl databases for *R. norvegicus*. The search parameters were the following: m/z accuracy for precursor and fragmented ions (5 ppm and 0.4 Da, respectively), fixed modification (carbamidomethylation [C]), and variable modifications (oxidation [M] and deamidation [N, Q]).

Quantitative analysis was performed manually using Xcalibur 3.0 (Thermo Scientific). The peak areas were integrated over the complete LC peaks in narrow mass windows (± 30 ppm around the peak center of the most abundant isotope peak, all isotope peaks with a cutoff at ~3% of relative abundance) for all charge states that appeared in the registered isotopic pattern for a given unique peptide. The analyzed peptides differentiate FLOP/FLIP variants of each subunit.

4.5. TaqMan analysis of transgene copy number

The TaqMan Copy Number Assay was applied to calculate the transgene copy number in TDP-43 TG rats. TaqMan MGB custom-made GFP and reference ubiquitin C (Rn01789812_g1) probes were used. Genomic DNA was extracted from ear tissue fragments using the Genomic Mini Kit (A&A Biotechnology), and real-time PCR was performed according to the manufacturer's instructions. Relative quantification of the transgene relative to a reference gene that is known to have two copies was performed.

4.6. Cue and context fear conditioning

Fear conditioning was performed in 6-month-old animals. The behavioral apparatus was described previously (Knapska et al., 2012). Briefly, observation chambers were situated in a sound-attenuating cabinet in an isolated room. The floor of the chambers consisted of stainless-steel rods that were wired to a shock source and solid-state grid scrambler (Med Associates) for footshock (US) delivery. A speaker was located on one wall of the chamber and used for presentation of the acoustic CS. Sensory stimuli were adjusted within these chambers to generate two different contexts (context A and context B). For context A, the individual chamber and room lights were on. The chambers were cleaned with a 1% ammonium hydroxide solution, and a few drops of the same solution were placed on pans below the grid floor to provide a distinct odor. Ventilation fans inside the cabinets supplied background noise (65 dB). The rats were transported to this context in transparent plastic cages. For context B, all of the room and chamber lights were off. Illumination was provided by 60 W red light bulbs. White Plexiglas floors were placed on the grid in each chamber. The chambers were cleaned with 1% acetic acid solution. A few drops of this solution were placed on pans below the grid floor before the animals were introduced. The rats were transported in black plastic boxes with bedding. Freezing behavior was recorded by a camera above each chamber.

On the first experimental day, the rats were placed in the chambers in context A. They were exposed to a single tone (30 s, 80 dB, 2 kHz) and footshock (2 s, 1 mA) during the last 2 s of tone presentation, 3 min after being placed in the chambers. Sixty seconds after the footshock, the rats were returned to their home cages. Twenty-four hours after the session, the rats were exposed to the tone in the novel context B. In context B, the CS was presented in the same manner as in context A with the same time intervals, but no US was presented. On the third day, the rats were reintroduced to context A with no CS or US presentations. Fear responses to the tone and context were assessed by measuring freezing behavior.

4.7. Pentylenetetrazole neuronal stimulation protocol

Pentylenetetrazole (50 mg/kg, i.p.) was used to evoke seizures in 7- to 8-month-old female rats. The animals were sacrificed 90 min after seizure induction. Only animals that reached a seizure level of 3.5–4, based on the modified Racine scale for PTZ-induced seizures (Luttjohann et al., 2009), were used for further studies. As controls, naive untreated rats were used. The animals were anesthetized, and tissue was processed according to the experimental protocol.

4.8. Dendritic spine visualization and analysis

For brain isolation, the rats were pre-sedated with an intraperitoneal injection of 75 mg/kg ketamine and 0.5 mg/kg medetomidine, deeply anesthetized with Morbital (150 mg/kg; 26.7 mg/ml pentobarbital, 133.3 mg/ml sodium pentobarbital), and transcardially perfused with ice-cold phosphate-buffered saline (PBS; pH 7.4) followed by 4% paraformaldehyde (PFA) in PBS (pH 7.4). Brains were removed and kept in ice-cold PBS until processing. For ballistic labeling, 300 µm serial coronal sections through the hippocampal formation were prepared on a vibratome (Leica). Lipofilic DiI (Invitrogen) was suspended in methylene chloride (Supelco) and spread on tungsten particles (Tungesten M-20, 1.3 µM, Bio-Rad). After drying, the particles were suspended in deionized water (R = 18.2 MΩ, Milli-Q, Millipore). Polyvinyl pyrrolidone (PVP, Sigma) was added, and the suspension was aspirated into Tefzel tubing (Bio-Rad) within a Tubing Prep Station (Bio-Rad) and rotated. After removing the PVP solution, the tubing was left rotating while being dried at increasing nitrogen LPM (liters per minute) flow values. Subsequently, the tubing was cut with a tubing cutter (Bio-Rad) into approximately 1 cm fragments and stored in the dark at room temperature.

For the tissue delivery of DiI-coated tungsten particles, a Helios Gene Gun (Bio-Rad) was used. Coronal brain sections (300 µm) were subjected to one bullet shot, resuspended in PBS, and left undisturbed to allow the dye to diffuse for approximately 2 h. Slices were post-fixed in 1.5% PFA for 48 h. The material was examined using a Leica TCS SP5 confocal microscope and Leica LAS AF software. Images from the stratum radiatum of the CA1 were collected using a 63× objective and the following parameters: 1024 × 1024 pixel count, 400 Hz frequency, 3.4× optical zoom. Z-stacks of dendrites were acquired at 0.42 µm and reconstructed using Fiji/ImageJ software. The images were analyzed using semiautomatic custom written Spine Magic software (Ruszczycki et al., 2012). The following spine parameters were analyzed: spine length, head width, neck width, spine circumference, and spine area.

4.9. Electrophysiological recordings

Electrophysiological experiments were performed using 6- to 8-month-old rats. Depending on the experimental protocol, brains were isolated from rats that were kept in control conditions or 90 min after PTZ-induced seizures.

4.10. Long-term potentiation

After isolation, brains were immersed in cold artificial cerebrospinal fluid (aCSF; 117 mM NaCl, 4.7 mM KCl, 2.5 mM $NaHCO_3$, 1.2 mM NaH_2PO_4, 2.5 mM $CaCl_2$, 1.2 mM $MgSO_4$, and 1 mM glucose, bubbled with carbogen) and cut into 400 µm coronal slices. Slices that contained the hippocampus were then transferred to a recording interface chamber (Harvard Apparatus) to recover at 33 °C ± 1 °C for at least 1.5 h before the LTP experiment began. The slices were continuously perfused with carbogenated aCSF at 33 °C ± 1 °C. fEPSPs were recorded from the stratum radiatum area of the CA1 area of the hippocampus using a glass pipette that was filled with 1 M NaCl (1–3 MΩ impendence). fEPSPs were evoked by stimulation of the Schaffer collateral-commissural every 30 s (test pulses at 0.033 Hz, 0.1 ms) using bipolar metal electrodes (FHC). The test stimulus intensity was adjusted to obtain fEPSPs with amplitudes that were one-half of the maximal response. After 15 min of stable baseline, LTP was induced tetanically (three trains of 100 Hz, 1-s stimulation at 3 min intervals). After the end of the HFS protocol, test pulses were subsequently applied for 90 min. Recordings were amplified (EX4–400, Dagan) and digitized (POWER 1401, CED). fEPSP slopes were analyzed online and offline using SIGNAL software (CED). For the analysis of LTP, the response slopes are expressed as a percentage of the average response slopes during the baseline period before LTP induction.

4.11. Neuronal excitability

Coronal brain slices, 300 µm thick, were prepared using a Leica VTS1000 vibratome in ice-cold NMDG cutting solution (135 mM NMDG, 1 mM KCl, 1.2 mM KH_2PO_4, 1.5 mM $MgCl_2{\cdot}6H_2O$, 0.5 mM $CaCl_2{\cdot}2H_2O$, 20 mM choline bicarbonate, and 10 mM D-glucose, bubbled with carbogene [5% CO_2, 95% O_2]). Slices that contained the hippocampus were collected, transferred to aCSF solution (119 mM NaCl, 2.5 mM KCl, 1 mM NaH_2PO_4, 26 mM $NaHCO_3$, 1.3 mM $MgCl_2$, 2.5 mM

$CaCl_2$, and 10 mM D-glucose), and incubated for at least 30 min at room temperature. The recording chamber was perfused with aCSF solution that was heated to 31 °C and constantly bubbled with carbogene. Hippocampal CA1 neurons were identified visually and patched with a borosilicate glass pipette at 4–6 MΩ resistance.

Recordings of action potentials were performed using potassium-based internal solution (120 mM K gluconate, 10 mM HEPES, 2 mM $MgCl_2$, 0.4 mM EGTA, 0.1 mM $CaCl_2$, 2.5 mM Na_2ATP, and 0.25 mM NaGTP, with the pH adjusted to 7.0–7.3 using KOH; 285–295 mOsm osmolarity). Series and input resistances were measured at the beginning and end of each recording. Action potentials were evoked by a single injection of a 500 ms step current, from −200 to 750 pA. The current was increased by 50 pA every 5 s. For kinetics measurements, only trains of action potentials from trials of five consecutive depolarizing steps between 300 and 600 pA were analyzed. These trains contained at least five action potentials.

4.12. mEPSC decay time

Voltage-clamp measurements were performed using cesium-based internal solution (130 mM Cs gluconate, 20 mM HEPES, 3 mM TEA-Cl, 0.4 mM EGTA, 4 mM Na2ATP, 0.3 mM NaGTP, and 4 mM QX-314Cl, pH 7.0–7.3; 290–295 mOsm osmolarity). Stable 5–10 min recording sweeps of mEPSCs were recorded and analyzed using Mini Analysis software. The mEPSC response decay time was measured between 90% and 10% of the peak amplitude. Cyclothiazide (Abcam) was dissolved in dimethylsulfoxide (DMSO), and a final concentration of 100 μM in an aCSF bath was applied. Equal volume of DMSO was added to aCSF for control cell recordings. Because action potentials were simultaneously recorded from the same slices, we avoided adding tetrodotoxin to the solution because the incomplete washout of tetrodotoxin can affect action potential measurements. Thus, the recorded mEPSCs were a mixture of miniature and spontaneous (action potential-driven) events.

4.13. Burst stimulation at 50 Hz

To evoke trains of EPSC responses, a bipolar AgCl electrode (inside a borosilicate two-barrel glass capillary that was filled with aCSF solution) was placed in the Shaffer collaterals. Nine 50-Hz TTL pulses of 0.2 ms were applied every 5 s, and postsynaptic responses were recorded from CA1 pyramidal cells. The aCSF solution contained DMSO and 50 μM picrotoxin. After 3–5 min of baseline recording, 50–100 stable sweeps of EPSCs were recorded. Afterward, aCSF that was supplemented with 100 μM CTZ was applied, and recordings were paused for 10 min to ensure the proper exchange of control aCSF with CTZ-containing aCSF. Recordings were then resumed, and 50–100 sweeps of trains of EPSCs were recorded. One cell per brain slice was recorded to avoid the incomplete washout of CTZ between recordings.

4.14. Statistical analysis

Student's *t*-test was used to compare measures between two groups. Two-way ANOVA followed by Fisher's Least Significant Difference post hoc test was used for comparisons between two groups under control conditions and upon PTZ and CTZ treatment. For data presentation, GraphPad Prism software was used. Values of $p < 0.05$ were considered statistically significant. All of the data were tested for normality using the Kolmogorov-Smirnov test.

Supplementary data to this article can be found online at https://doi.org/10.1016/j.nbd.2019.104499.

Acknowledgements

We thank Dr. Jane Wu (Northwestern University, Feinberg School of Medicine, Chicago, IL USA) for providing the hTDP-43–eGFP fusion construct. This study was supported by National Science Centre (SONATA) grant UMO-2011/01/D/NZ4/03744 and the ANIMOD project within the Team Tech Core Facility Plus program of the Foundation for Polish Science, co-financed by the European Union under the European Regional Development Fund to WK. The MS analysis was performed at the Mass Spectrometry Laboratory, Institute of Biochemistry and Biophysics, Polish Academy of Sciences, and at the Biological and Chemical Research Centre, University of Warsaw, established within a project that was co-financed by the European Union from the European Regional Development Fund under the Operational Programme Innovative Economy 2007-2013.

References

Aizawa, H., et al., 2010. TDP-43 pathology in sporadic ALS occurs in motor neurons lacking the RNA editing enzyme ADAR2. Acta Neuropathol. 120, 75–84.
Arai, A.C., Kessler, M., 2007. Pharmacology of ampakine modulators: from AMPA receptors to synapses and behavior. Curr. Drug Targets 8, 583–602.
Arai, A., Lynch, G., 1998. The waveform of synaptic transmission at hippocampal synapses is not determined by AMPA receptor desensitization. Brain Res. 799, 230–234.
Avendano-Vazquez, S.E., et al., 2012. Autoregulation of TDP-43 mRNA levels involves interplay between transcription, splicing, and alternative polyA site selection. Genes Dev. 26, 1679–1684.
Ayala, Y.M., et al., 2011. TDP-43 regulates its mRNA levels through a negative feedback loop. EMBO J. 30, 277–288.
Balik, A., et al., 2013. Activity-regulated RNA editing in select neuronal subfields in hippocampus. Nucleic Acids Res. 41, 1124–1134.
Benke, T.A., et al., 1998. Modulation of AMPA receptor unitary conductance by synaptic activity. Nature. 393, 793–797.
Bieganska, K., et al., 2012. Silencing of ICERs (inducible cAMP early repressors) results in partial protection of neurons from programmed cell death. Neurobiol. Dis. 45, 701–710.
Bose, J.K., et al., 2008. TDP-43 overexpression enhances exon 7 inclusion during the survival of motor neuron pre-mRNA splicing. J. Biol. Chem. 283, 28852–28859.
Buratti, E., Baralle, F.E., 2012. TDP-43: gumming up neurons through protein-protein and protein-RNA interactions. Trends Biochem. Sci. 37, 237–247.
Buratti, E., et al., 2004. Nuclear factor TDP-43 binds to the polymorphic TG repeats in CFTR intron 8 and causes skipping of exon 9: a functional link with disease penetrance. Am. J. Hum. Genet. 74, 1322–1325.
Cais, O., et al., 2014. Mapping the interaction sites between AMPA receptors and TARPs reveals a role for the receptor N-terminal domain in channel gating. Cell Rep. 9, 728–740.
Chen, C., et al., 2002. Contributions of receptor desensitization and saturation to plasticity at the retinogeniculate synapse. Neuron. 33, 779–788.
Chiang, P.M., et al., 2010. Deletion of TDP-43 down-regulates Tbc1d1, a gene linked to obesity, and alters body fat metabolism. Proc. Natl. Acad. Sci. U. S. A. 107, 16320–16324.
Cohen, S., Greenberg, M.E., 2008. Communication between the synapse and the nucleus in neuronal development, plasticity, and disease. Annu. Rev. Cell Dev. Biol. 24, 183–209.
Coleman, S.K., et al., 2010. Ligand-binding domain determines endoplasmic reticulum exit of AMPA receptors. J. Biol. Chem. 285, 36032–36039.
Constals, A., et al., 2015. Glutamate-induced AMPA receptor desensitization increases their mobility and modulates short-term plasticity through unbinding from Stargazin. Neuron. 85, 787–803.
Daoudal, G., Debanne, D., 2003. Long-term plasticity of intrinsic excitability: learning rules and mechanisms. Learn. Mem. 10, 456–465.
Dong, H., et al., 2014. Curcumin abolishes mutant TDP-43 induced excitability in a motoneuron-like cellular model of ALS. Neuroscience. 272, 141–153.
Figiel, I., Kaczmarek, L., 1997. Cellular and molecular correlates of glutamate-evoked neuronal programmed cell death in the in vitro cultures of rat hippocampal dentate gyrus. Neurochem. Int. 31, 229–240.
Fioravante, D., Regehr, W.G., 2011. Short-term forms of presynaptic plasticity. Curr. Opin. Neurobiol. 21, 269–274.
Freibaum, B.D., et al., 2010. Global analysis of TDP-43 interacting proteins reveals strong association with RNA splicing and translation machinery. J. Proteome Res. 9, 1104–1120.
Fucile, S., et al., 2006. Effects of cyclothiazide on GluR1/AMPA receptors. Proc. Natl. Acad. Sci. U. S. A. 103, 2943–2947.
Gautam, M., et al., 2019 Jan. Mitochondria, ER, and nuclear membrane defects reveal early mechanisms for upper motor neuron vulnerability with respect to TDP-43 pathology. Acta Neuropathol. 137 (1), 47–69. https://doi.org/10.1007/s00401-018-1934-8.
Granger, R., et al., 1993. A drug that facilitates glutamatergic transmission reduces exploratory activity and improves performance in a learning-dependent task. Synapse. 15, 326–329.
Hampson, R.E., et al., 1998. Facilitative effects of the ampakine CX516 on short-term memory in rats: correlations with hippocampal neuronal activity. J. Neurosci. 18, 2748–2763.
Heine, M., et al., 2008. Surface mobility of postsynaptic AMPARs tunes synaptic transmission. Science. 320, 201–205.
Igaz, L.M., et al., 2011. Dysregulation of the ALS-associated gene TDP-43 leads to neuronal death and degeneration in mice. J. Clin. Invest. 121, 726–738.

Ingvar, M., et al., 1997. Enhancement by an ampakine of memory encoding in humans. Exp. Neurol. 146, 553–559.
Kandel, E.R., et al., 2014. The molecular and systems biology of memory. Cell. 157, 163–186.
Kim, J.J., Fanselow, M.S., 1992. Modality-specific retrograde amnesia of fear. Science. 256, 675–677.
Knapska, E., et al., 2012. Functional anatomy of neural circuits regulating fear and extinction. Proc. Natl. Acad. Sci. U. S. A. 109, 17093–17098.
Konopka, W., et al., 2010. MicroRNA loss enhances learning and memory in mice. J. Neurosci. 30, 14835–14842.
Konopka, W., et al., 2011. The microRNA contribution to learning and memory. Neuroscientist. 17, 468–474.
La Via, L., et al., 2013. Modulation of dendritic AMPA receptor mRNA trafficking by RNA splicing and editing. Nucleic Acids Res. 41, 617–631.
Lomeli, H., et al., 1994. Control of kinetic properties of AMPA receptor channels by nuclear RNA editing. Science. 266, 1709–1713.
Luttjohann, A., et al., 2009. A revised Racine's scale for PTZ-induced seizures in rats. Physiol. Behav. 98, 579–586.
Lynch, G., Gall, C.M., 2006. Ampakines and the threefold path to cognitive enhancement. Trends Neurosci. 29, 554–562.
Lynch, G., et al., 1996. Psychological effects of a drug that facilitates brain AMPA receptors. Int. Clin. Psychopharmacol. 11, 13–19.
Majumder, P., et al., 2012. TDP-43 regulates the mammalian spinogenesis through translational repression of Rac1. Acta Neuropathol. 124, 231–245.
Matsuzaki, M., et al., 2004. Structural basis of long-term potentiation in single dendritic spines. Nature. 429, 761–766.
Mercado, P.A., et al., 2005. Depletion of TDP 43 overrides the need for exonic and intronic splicing enhancers in the human apoA-II gene. Nucleic Acids Res. 33, 6000–6010.
Mitsushima, D., et al., 2011. Contextual learning requires synaptic AMPA receptor delivery in the hippocampus. Proc. Natl. Acad. Sci. U. S. A. 108, 12503–12508.
Mosbacher, J., et al., 1994. A molecular determinant for submillisecond desensitization in glutamate receptors. Science. 266, 1059–1062.
Neumann, M., et al., 2006. Ubiquitinated TDP-43 in frontotemporal lobar degeneration and amyotrophic lateral sclerosis. Science. 314, 130–133.
Ostroff, L.E., et al., 2010. Fear and safety learning differentially affect synapse size and dendritic translation in the lateral amygdala. Proc. Natl. Acad. Sci. U. S. A. 107, 9418–9423.
Ou, S.H., et al., 1995. Cloning and characterization of a novel cellular protein, TDP-43, that binds to human immunodeficiency virus type 1 TAR DNA sequence motifs. J. Virol. 69, 3584–3596.
Partin, K.M., et al., 1994. Cyclothiazide differentially modulates desensitization of alpha-amino-3-hydroxy-5-methyl-4-isoxazolepropionic acid receptor splice variants. Mol. Pharmacol. 46, 129–138.
Partin, K.M., et al., 1996. AMPA receptor flip/flop mutants affecting deactivation, desensitization, and modulation by cyclothiazide, aniracetam, and thiocyanate. J. Neurosci. 16, 6634–6647.
Pei, W., et al., 2009. Flip and flop: a molecular determinant for AMPA receptor channel opening. Biochemistry 48, 3767–3777.
Penn, A.C., et al., 2012. Activity-mediated AMPA receptor remodeling, driven by alternative splicing in the ligand-binding domain. Neuron. 76, 503–510.
Penn, A.C., et al., 2017. Hippocampal LTP and contextual learning require surface diffusion of AMPA receptors. Nature. 549, 384–388.
Polymenidou, M., et al., 2011. Long pre-mRNA depletion and RNA missplicing contribute to neuronal vulnerability from loss of TDP-43. Nat. Neurosci. 14, 459–468.
Ruszczycki, B., et al., 2012. Sampling issues in quantitative analysis of dendritic spines morphology. BMC Bioinform. 13, 213.
Sephton, C.F., et al., 2010. TDP-43 is a developmentally regulated protein essential for early embryonic development. J. Biol. Chem. 285, 6826–6834.
Sephton, C.F., et al., 2011. Identification of neuronal RNA targets of TDP-43-containing ribonucleoprotein complexes. J. Biol. Chem. 286, 1204–1215.
Sommer, B., et al., 1990. Flip and flop: a cell-specific functional switch in glutamate-operated channels of the CNS. Science. 249, 1580–1585.
Sun, M., et al., 2017. Cryptic exon incorporation occurs in Alzheimer's brain lacking TDP-43 inclusion but exhibiting nuclear clearance of TDP-43. Acta Neuropathol. 133, 923–931.
Swarup, V., et al., 2011. Pathological hallmarks of amyotrophic lateral sclerosis/frontotemporal lobar degeneration in transgenic mice produced with TDP-43 genomic fragments. Brain. 134, 2610–2626.
Taschenberger, H., et al., 2002. Optimizing synaptic architecture and efficiency for high-frequency transmission. Neuron. 36, 1127–1143.
Tollervey, J.R., et al., 2011. Characterizing the RNA targets and position-dependent splicing regulation by TDP-43. Nat. Neurosci. 14, 452–458.
Wang, I.F., et al., 2008. TDP-43, the signature protein of FTLD-U, is a neuronal activity-responsive factor. J. Neurochem. 105, 797–806.
Wils, H., et al., 2010. TDP-43 transgenic mice develop spastic paralysis and neuronal inclusions characteristic of ALS and frontotemporal lobar degeneration. Proc. Natl. Acad. Sci. U. S. A. 107, 3858–3863.
Wu, L.S., et al., 2010. TDP-43, a neuro-pathosignature factor, is essential for early mouse embryogenesis. Genesis 48, 56–62.
Wu, L.S., et al., 2012. Targeted depletion of TDP-43 expression in the spinal cord motor neurons leads to the development of amyotrophic lateral sclerosis-like phenotypes in mice. J. Biol. Chem. 287, 27335–27344.
Xiao, S., et al., 2011. RNA targets of TDP-43 identified by UV-CLIP are deregulated in ALS. Mol. Cell. Neurosci. 47, 167–180.
Xu, Y.F., et al., 2010. Wild-type human TDP-43 expression causes TDP-43 phosphorylation, mitochondrial aggregation, motor deficits, and early mortality in transgenic mice. J. Neurosci. 30, 10851–10859.
Yamada, K.A., 1998. Modulating excitatory synaptic neurotransmission: potential treatment for neurological disease? Neurobiol. Dis. 5, 67–80.
Yang, Y., et al., 2008. Spine expansion and stabilization associated with long-term potentiation. J. Neurosci. 28, 5740–5751.
Yang, C., et al., 2014. Partial loss of TDP-43 function causes phenotypes of amyotrophic lateral sclerosis. Proc. Natl. Acad. Sci. U. S. A. 111, E1121–E1129.
Zhou, M., et al., 2009. Fear conditioning enhances spontaneous AMPA receptor-mediated synaptic transmission in mouse hippocampal CA1 area. Eur. J. Neurosci. 30, 1559–1564.